PLANAR DEFECTS IN SILICON

Progress Report

H. Föll

D. Ast

In the time period from January 1977 to June 1978 research has been conducted in the following areas:

i) establishing welding procedures for Si crystals in order to produce geometrically well-defined boundaries

ii) transmission electron microscopy (TEM) characterization of the boundaries thus produced

iii) characterization of defects in EFG Si ribbons by

- TEM
- scanning electron microscopy in the electron-beam induced current (EBIC) mode
- chemical etching

Most efforts have been concentrated on *i*); this report however will emphasize *iii*).

I. General Remarks to Structural and Electronic Properties of Defects in Semiconductors

An understanding of defects exhibiting "electronic properties" requires a knowledge of their influence on the band structure of a semiconductor. Defects usually introduce one or more energy levels in the gap and may, if present in large concentrations, in addition change the band structure itself, e.g. alter the band gap. Despite numerous efforts a detailed knowledge of energy levels of most lattice defects larger than point defects has not yet been achieved, although reliable data seem to emerge for dislocations (see, e.g. |1|). The remarkable state of confusion found when scanning the literature is closely related to the still rather poor understanding of structural defect properties in semiconductors; the recent discussion about the dissociation of dislocations into partials , e.g. |2|, may serve as an example.

In the case of planar defects, particularly for stacking faults and and twin boundaries, it is still presently not clear whether these faults in their "clean" state are electrically active or whether the observed electronic properties are due to secondary effects as, e.g., impurity segregation. Similarly, in the case of high-angle grain boundaries it is not known if their electronic properties are due to the secondary dislocations, which are believed to be an integral part of their equilibrium structure |3|, or caused by the boundary interface itself. In the first case one would expect the electronic properties to be very sensitive to small changes in any one of the five parameters describing the geometry of the boundary since the density of secondary dislocation varies drastically with these parameters; in the second case no such effects would be expected. Ledges, extrinsic dislocations or impurity segregation in the boundary may additionally obscure the interpretation of experimental results.

To our knowledge, no detailed structural characterization of grain boundaries in semiconductors has been carried out to date. The few existing electronic measurements (e.g. |4|) are therefore difficult to relate to specific structures and can only be explained in very general terms.

We approached the structural characterization of grain boundaries in two different ways: *i*) Production and detailed structural characterization of geometrically well-defined grain boundaries obtained by a welding technique, and *ii*) Compariative investigations of as-grown boundaries in Si ribbons by etching, EBIC and TEM.

II. Brief Review of Results Obtained from Welded Boundaries

2.1 The Welding Process

Welding in an H_2-atmosphere at ~ 1250°C, with a small pressure on the specimens to be welded, proved to generate good boundaries. Generally, the boundaries produced by this technique contain amorphous precipitates; we believe that these might be the remainders of the SiO_2-layer originally covering the specimen surfaces.

2.2 Results

The following boundaries have been produced:

i) low-angle twist boundaries on {100} planes

ii) low-angle twist boundaries on {111} planes

iii) twin boundaries on {111} planes

Figure 1 shows typical examples of observed boundary structures. The {100} twist boundary exhibits a square network of $b = \frac{a}{2}$ <100> screw dislocations in accordance with theory. The boundaries on {111} planes show a hexagonal network of screw dislocations ($\underline{b} = \frac{a}{2}$ <110> and $\underline{b} = \frac{a}{6}$ <112> for the low-angle or twin boundary, respectively), which is, however, degenerated into a network of extended dislocation nodes containing extrinsic and intrinsic stacking faults (in the picture shown, only intrinsic stacking faults are in good contrast).

So far, the boundaries generated behave exactly like the corresponding boundaries in fcc metals. Complications can be expected for boundaries with particular Σ*) values |5|. The grain boundaries in Si obtained by welding proved to be well suited to study grain boundaries in general and offer considerable advantages over the usual use of metal crystals. This is due to the following unique features characteristic for Si (or Ge): *i*) large dislocation-free crystals can be prepared with high-quality surfaces of any given orientation; any kind of boundary thus can be easily produced by welding. *ii*) A large lattice constant (a = 5.4 Å) enables fairly easy access to direct lattice imaging techniques which extend the range of conventional TEM to an atomic level. *iii*) The immobility of dislocations in Si below ~ 200°C conserves the boundary structures during specimen preparation, no artifacts due to thinning and free surfaces near the defects have to be encountered. *iv*) The high points stresses in Si tend to enhance the regularity of networks even at large spacings. This is an important point for developing diffraction techniques from grain boundaries to a level where they can be used to characterize boundaries with no detectable structures. In addition to *i*)-*iv*), producing

---

*) for definition of Σ see |3|

boundaries with particular properties can in turn give valuable information about basic defect properties in Si, see below.

Figures 2-5 give selected examples of the aforesaid. Figure 2 shows direct lattice images of a low-angle twist boundary and a low-angle tilt boundary. Dislocations- and stacking faults are clearly visible; the amount of detailed information contained in these micrographs could not be obtained with any other technique. Figure 3 shows direct lattice-fringe images of one set of the screw dislocations in a {100} low-angle twist boundary. It appears that the core width of the dislocations decreases with decreasing spacing, contrary to the theoretical prediction |6|. Figure 4 shows the diffraction spots produced by the dislocation of a {100} twist boundary*) in the vicinity of matrix spots. Due to the well-defined geometry of the sample and the regularity of the network (e.g. Fig. 1) double-diffraction effects, usually obscruing the interpretation of diffraction patterns from grain boundaries, can be sorted out easily. Figure 5 shows a so-called "double ribbon", formed under certain circumstances in {111} twist boundaries. Double ribbons allow the most accurate determination of the stacking fault energies of both, intrinsic and extrinsic stacking fault energies of all methods known so far. The values obtained were $\gamma_{in} = 100 \pm$ mJm^{-2} and $\gamma_{in} : \gamma_{ex} = 1.16 \pm 0.1$. These results, obtained for the first time with the double ribbon method in Si, not only seriously question earlier results |7|, but shed some serious doubts on the accuracy of the standard methods used to determine stacking fault energies.

III. Silicon Ribbons

All experiments reported here were done with uncharacterized ribbon pieces grown by IBM via edge defined film growth (EFG). The main intention was to develop standard methods for defect characterization and to establish a classification scheme for the defect structure and the over-all quality of a ribbon.

3.1 Projected Course of Investigations

---

*) The help of C. B. Carter, who supplied this picture is gratefully acknowledged.

Our way of characterizing the defect sturcture of ribbons will be as follows:

As-grown ribbons are first cut into suitable pieces and subsequently prepared for chemical etching. This usually includes grinding, lapping and polishing of one or both surfaces. The specimens are then etched for 20-30 seconds. The defect structure revealed by the etching procedure is recorded, and particularly interesting areas are selected for further investigations.

Schottky contacts are then made and the electronic properties of the specimens are probed by EBIC. A comparison with the etching patterns thus reveals the defects of special interest.

The specimens (at this stage typically 10 mm x 10 mm) are then cut into smaller pieces suitable for TEM (typically 2.5 x 2.5 mm) and thinned, either chemically, by ion-milling or by a combination of both.

A full characterization of one specimen with all the techniques mentioned above has not yet been aspired. Emphasis was put was put instead on the development of these techniques to a point where they can be used routinely. It is our belief that this procedure not only allows a quick and through characterization of ribbons at large (especially after interpretations of etching patterns are possible on a large scale because of feedback from EBIC and TEM) but also allows basic studies of electronic defect properties in the course outlined before.

2.2 Details of Experimental Methods and First Results

Etching techniques for Si are well known and developed over the years from a somewhat black art to a sophisticated and valuable tool for defect characterization. The interpretation of etching patterns produced by boundaries, however, is not too well established compared to dislocations and point defect clusters. The interpretation of boundary etching structures at the beginning thus need considerable feed-back from TEM.

We developed a preparation technique which allow us to have the defect of interest (as related by etching) within the thin area of a TEM sample. This can be achieved by chemically thinning the specimen until a small hole appears. The size of the hole is then slowly increased

by either chemically thinning with a "slow" solution or by ion-milling under optical control. The final stage is arrived when the edge of the hole cuts through the defect. Figure 6 shows a specimen before and after thinning; it can be seen that the interesting defect (the "wedge" within the twin boundaries) is partially contained within the thin specimen areas near the edge of the hole. TEM investigations then demonstrated that the "wedge" is formed by a number of wavily facetted incoherent twin boundaries on mainly {112} planes. Other defects detailedly characterized with this technique are microtwins ending in the specimen and secondary twins. After the "calibration" of the etching features by TEM is completed it is hoped to identify certain defects only by etching.

EBIC work so far was mainly concerned with finding reliable methods for the production of Schottky diodes. The properties of Si-metal interfaces which control the properties of the diodes are generally not well known. Since theoretical prediction about particular systems are not reliable, the best combinations have to be found experimentally. It appears that a thermal evaporation of Ti after a short $HF:HNO_3$ etch [8] provides satisfactory diodes, but other promising systems are, e.g., sputter deposition of Pd, are also being investigated.

A direct comparison between etching structures and EBIC pictures would be greatly facilitated if Schottky diodes could be made on etched surfaces without producing EBIC contrast artifacts. A comparison etching - EBIC could then be made by simply switching from the SEM-mode to the EBIC mode of the microscope. Preliminary results are promising; an example is given in Fig. 7.

The EBIC results obtained so far demonstrate that dislocation and grain boundaries are generally electrically active; i.e. reduce the collection efficiency of the diode. Coherent twin boundaries are not necessarily active; if they are, their activity is related to defects within or nearby the boundary. At present it is not clear how electronic activity is related to the various defect structures observed in twin boundaries (see below).

TEM studies have also been carried out with samples randomly selected from ribbon material which was not pre-characterized by etching. The overwhelming majority of the

defects observed was found to be ensembles of parallel running coherent twin boundaries, thus forming microtwins with respect to a matrix orientation. Direct lattice imaging proved that these twin boundaries are absolutely perfect and are not decorated with precipitates $\gtrsim$ 10 Å as shown by the absence of Moiré contrast, see Fig. 8. Sometimes twinning dislocations ($\underline{b} = \frac{a}{6}$ <112>) are observed, the most interesting observations are however microtwins changing their thickness or ending in the specimen. This was observed to take place with three different mechanisms: *i*) by arrays of twinning dislocations ($\underline{b} = \frac{a}{6}$ <112> or $\underline{b} = \frac{a}{3}$ <111>); interaction between these dislocations can lead to emission of lattice dislocations (Sleeswky mechanism |9|), the microtwin in this case acts as a dislocation source, see Fig. 9. *ii*) by the formation of incoherent twin boundaries on {112} planes. A lattice image and a schematic drawing of this case is shown in Fig. 10. In Fig. 10 the microtwin only decreases its width, but microtwins ending in the specimen with precisely the same mechanism have also been observed. As an interesting side observation it may be mentioned that this lattice image directly shows the existence of rigid-body translations the boundary, a hypothesis suggested by in |10|. *iii*) by emitting planar defects, see Fig. 11, possibly stacking faults or secondary microtwins. The detailed nature of these defects is still unclear and requires further studies. Other defects frequently observed are incoherent twin boundaries, low angle grain boundaries or dislocation arrays (Fig. 12) and high-angle grain boundaries. Besides boundaries clearly exhibiting a secondary dislocation network (Fig. 13) "structureless" boundaries have also been observed. An investigation whether those boundaries are truly amorphous or still crystalline with structures below the resolution limit of TEM requires sophisticated diffraction techniques and is currently underway.

A general impression from the work performed so far is that many defects besides twin and high-angle grain boundaries are not directly grown-in from the melt but generated as a result of plastic deformation during the cooling cycle of the ribbons.

Acknowledgments

Many fruitful discussions with and valuable experimental help of C. B. Carter are gratefully acknowledged. Drs. T. Sullivan and J. Gambino contributed to part III of this paper; their help is greated appreciated.

This work was supported by DOE.

REFERENCES

|1| R. Labusch, W. Schröter, (1975). Inst. Phys. Conf. Ser. No. 23, p. 56.

|2| H. Föll and C. B. Carter, to be published.

|3| W. Bollmann, (1970), Crystal Defects and Crystalline Interfaces, Springer Verlag, New York.

|4| H. F. Mataré (1971), Defect Electronics in Semiconductors, Wiley Interscience, New York.

|5| W. Bollmann, private communication.

|6| P. H. Pumphrey, H. Gleiter, P. J. Goodhew, (1977), Phil. Mag. 36, 1099.

|7| A. Gomez, D. J. H. Cockayne, P. B. Hirsch, V. Vitek, (1974), Phil. Mag. 31, 105.

|8| L. C. Kimmerling, H. J. Leamy, J. L. Benton, S. D. Ferris, P. E. Freeland and J. J. Rubin, (1977), Semiconductor Silicon, eds. H. H. Huff and E. Sirtl, The Electrochemical Society, Inc., p. 468.

|9| A. W. Sleeswky, (1962), Acta. Met. 10, 705.

|10| R. C. Pond, V. Vitek, (1977), Proc. R. Soc. London A. 357, 453.

Fig. 1

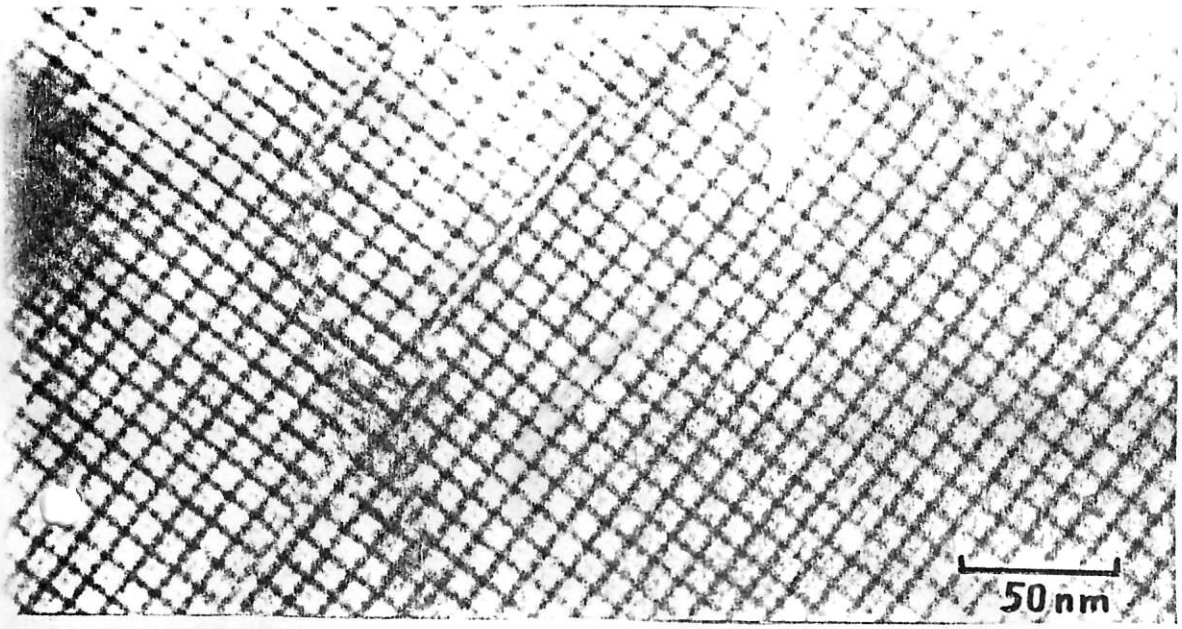

low - angle twi
boundary
on {100}

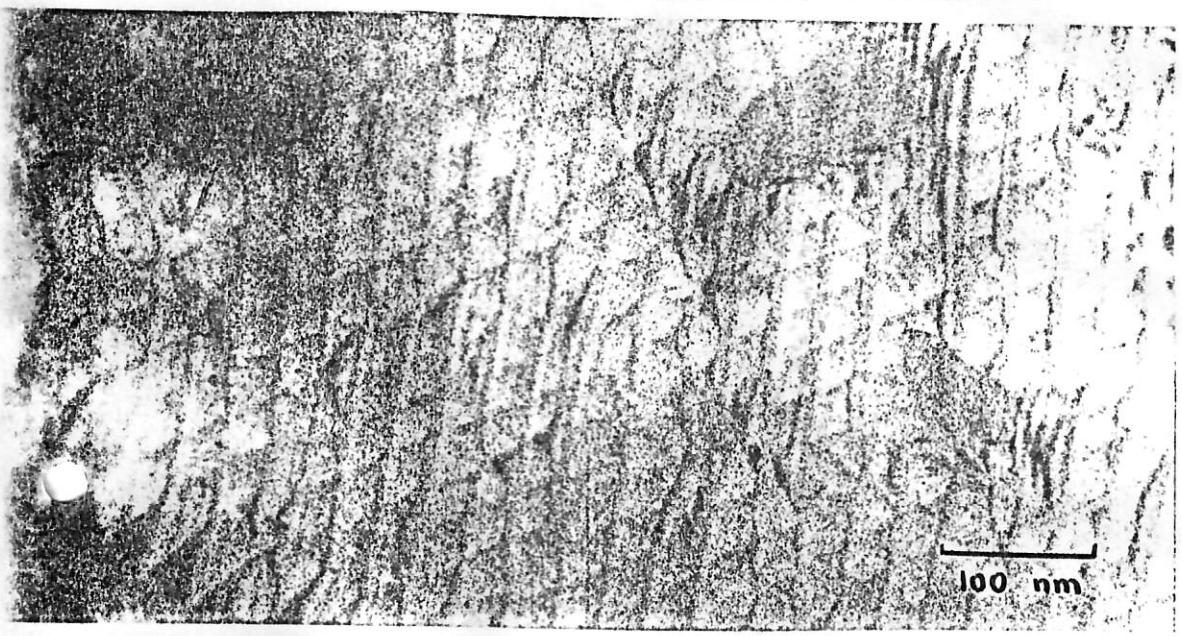

low - angle twi
boundary
on {111}

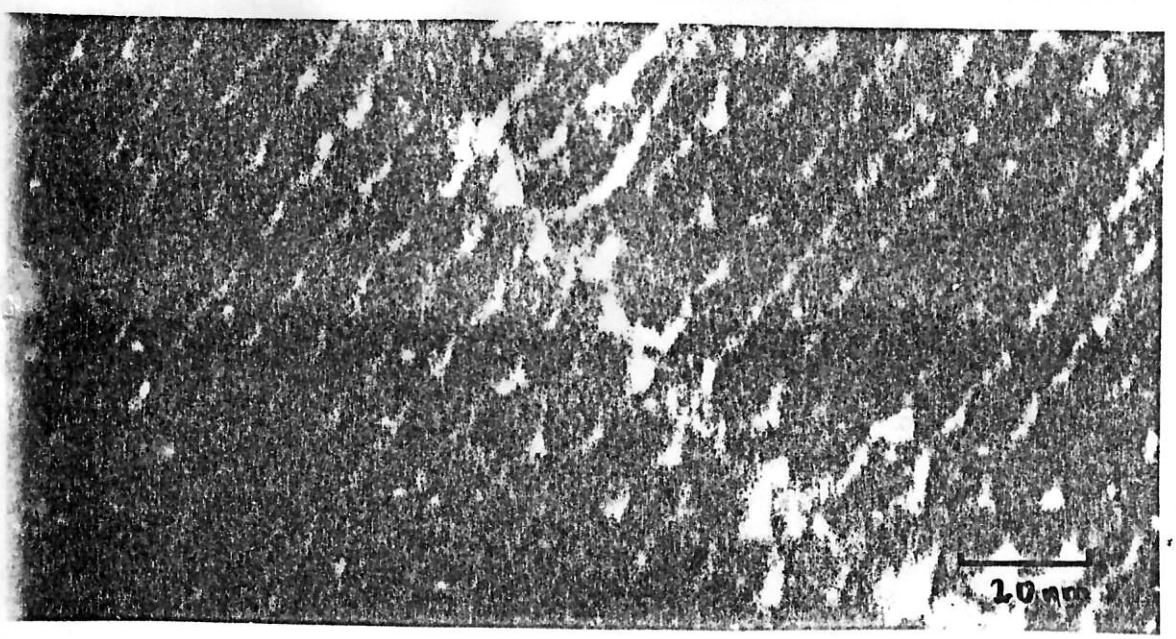

twin with addi
twist on {111}

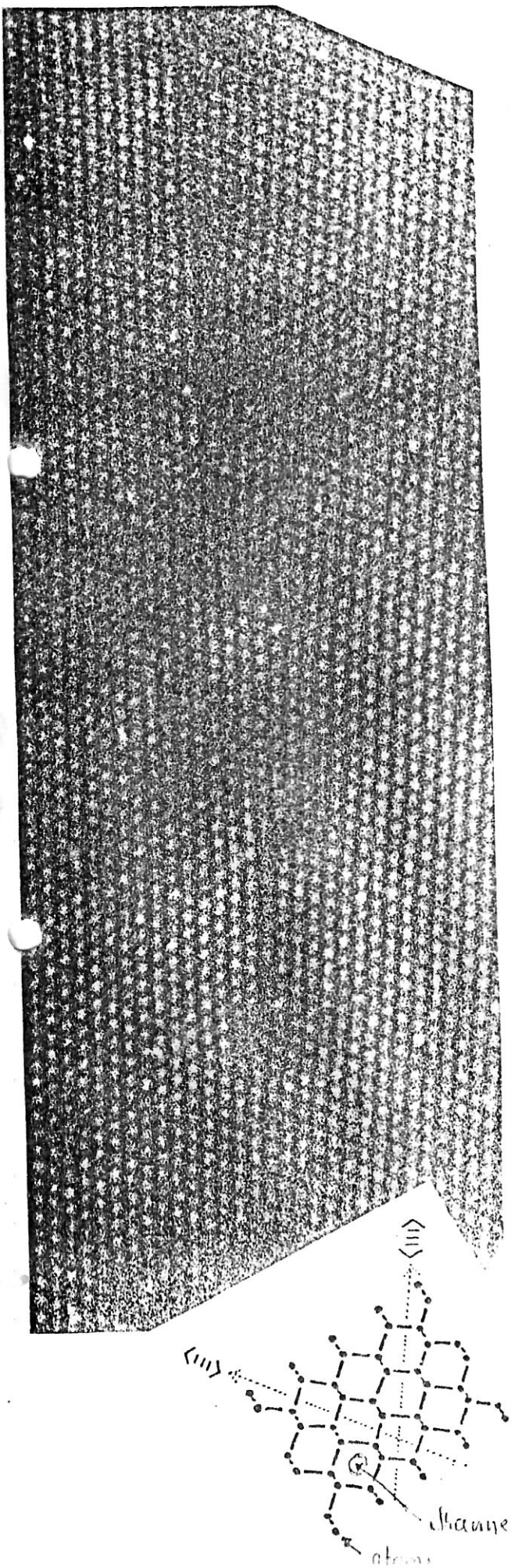

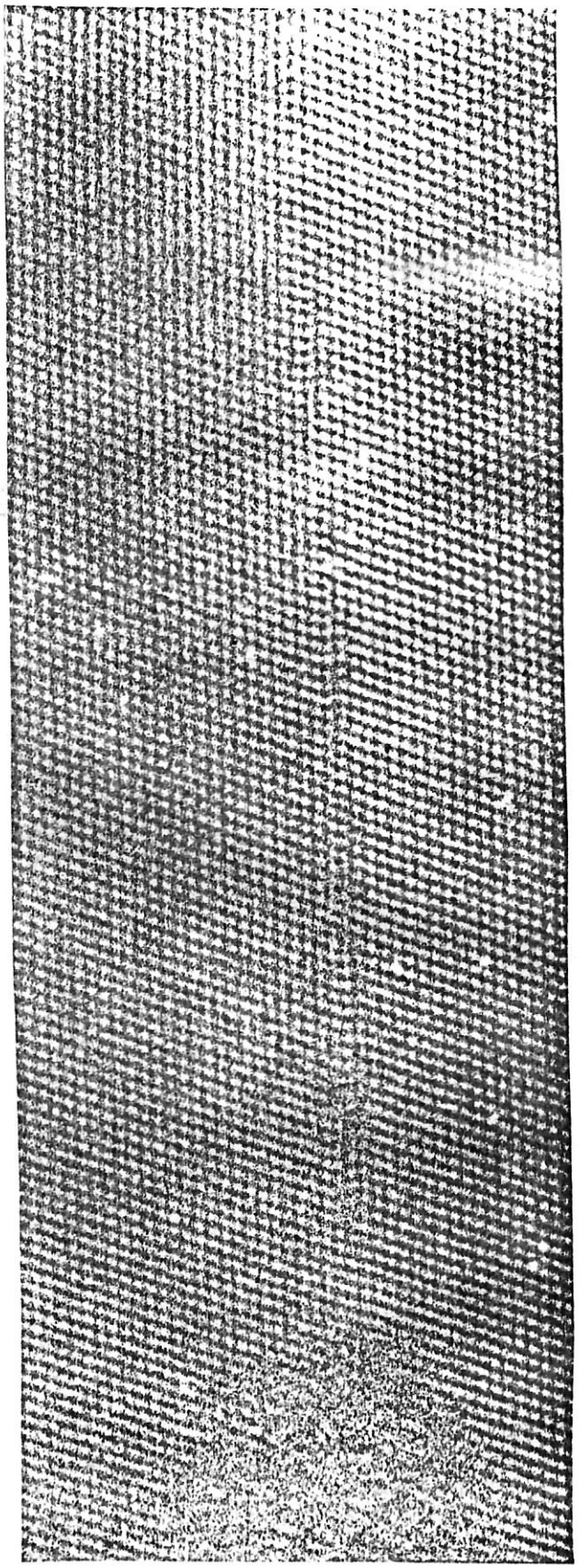

Fig. 2 Small-angle tilt (left) and twist boundary. The ins shows the projected lattice str along ⟨110⟩. White dots in the i correspond to channels.

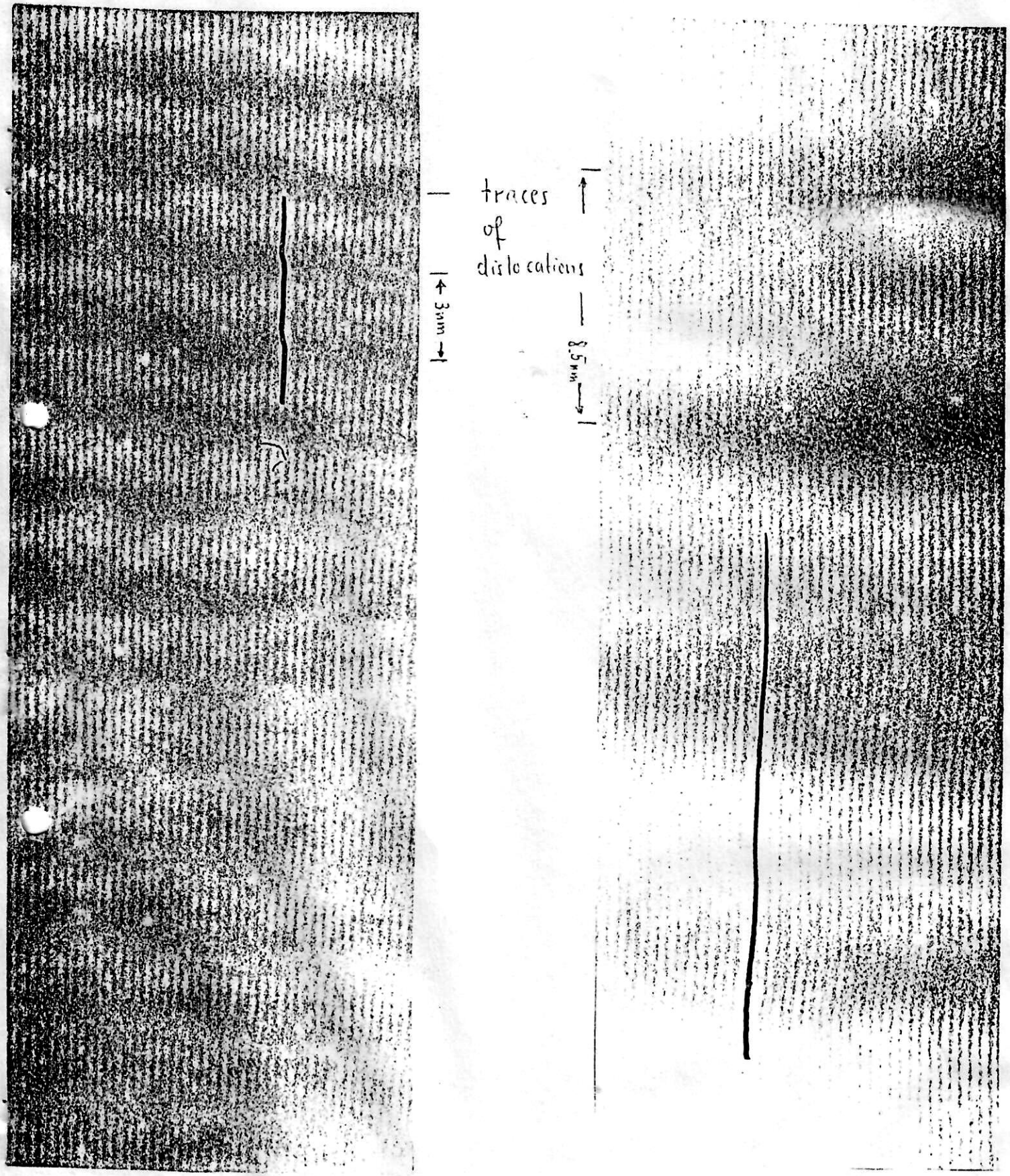

Fig. 3 Lattice fringe image of screw dislocations in a low-angle twist boundary on {100}. Only one set of dislocations shows up.

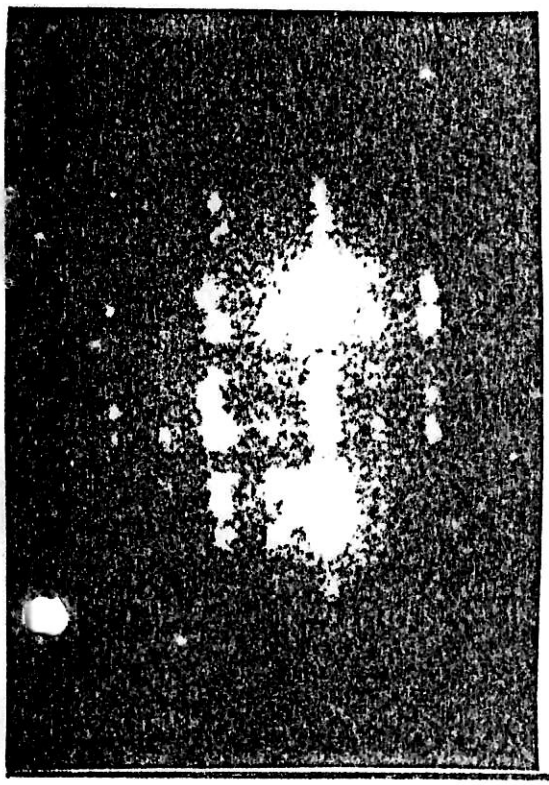

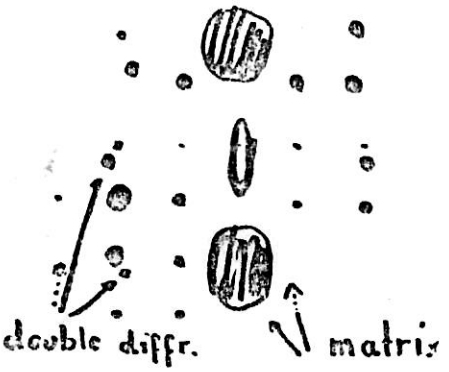

Fig. 4

Diffraction pattern from dislocation network in small angle twist boundary on

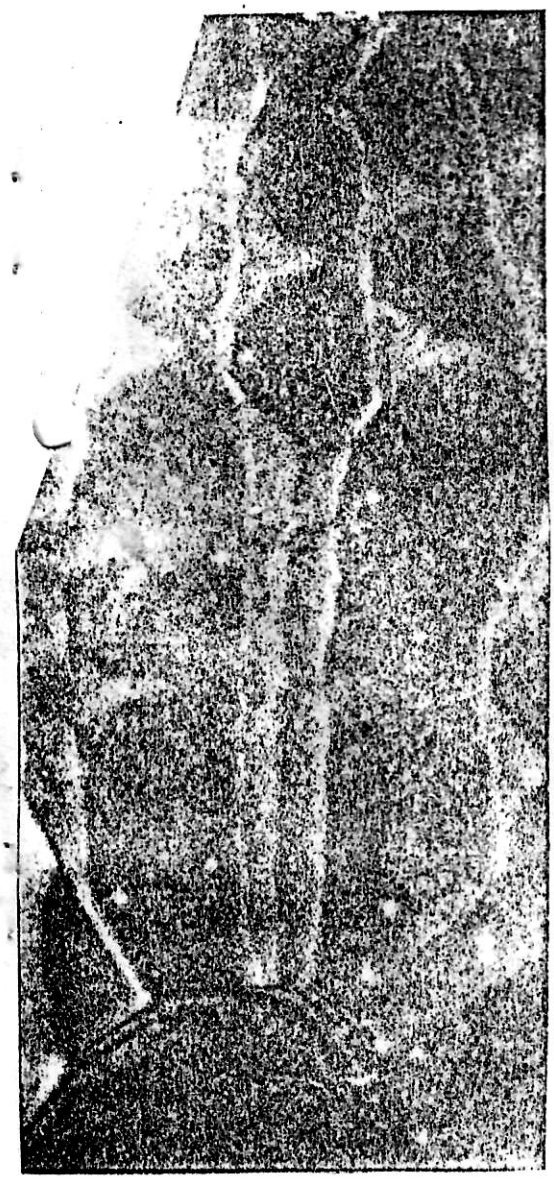

Fig. 5

Double ribbon and its geometry

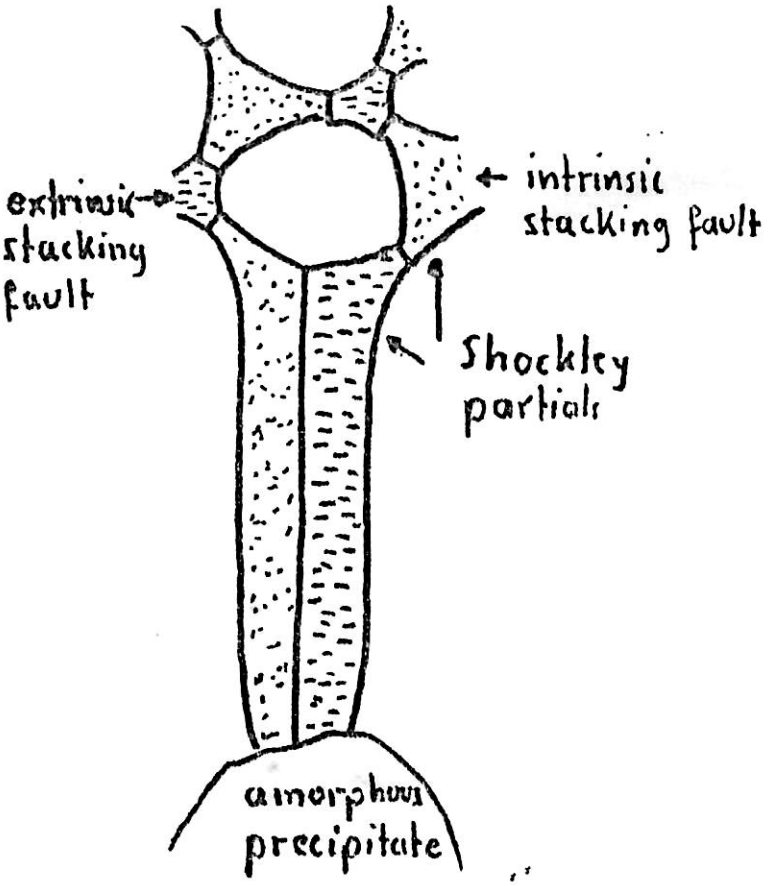

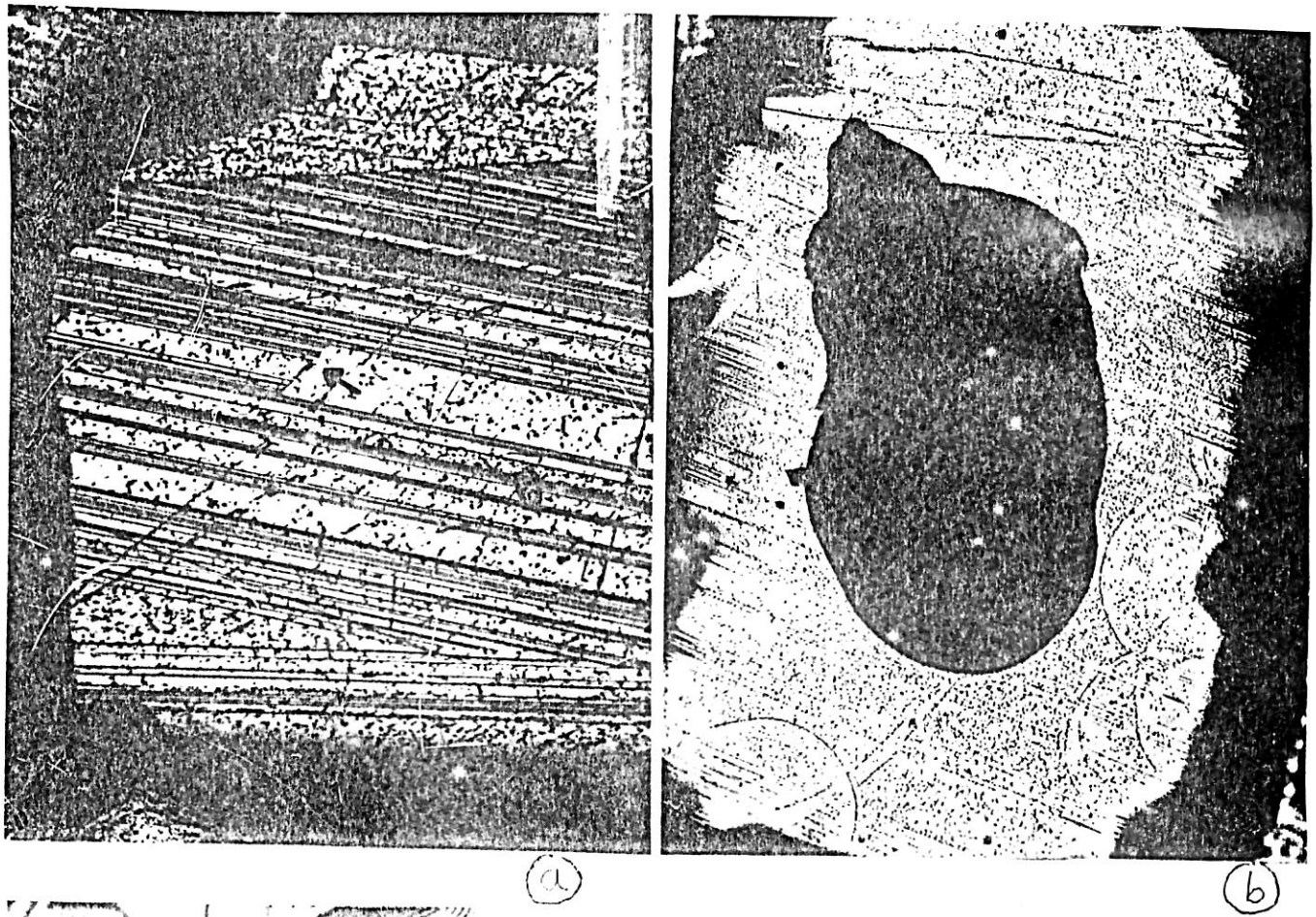

Fig. 6 a) Etch pattern before thinning } Defect marked with arrow
b) Etch pattern after thinning }
c) TEM micrograph showing incoherent twin boundaries and coherent twin boundaries (marked with arrow)

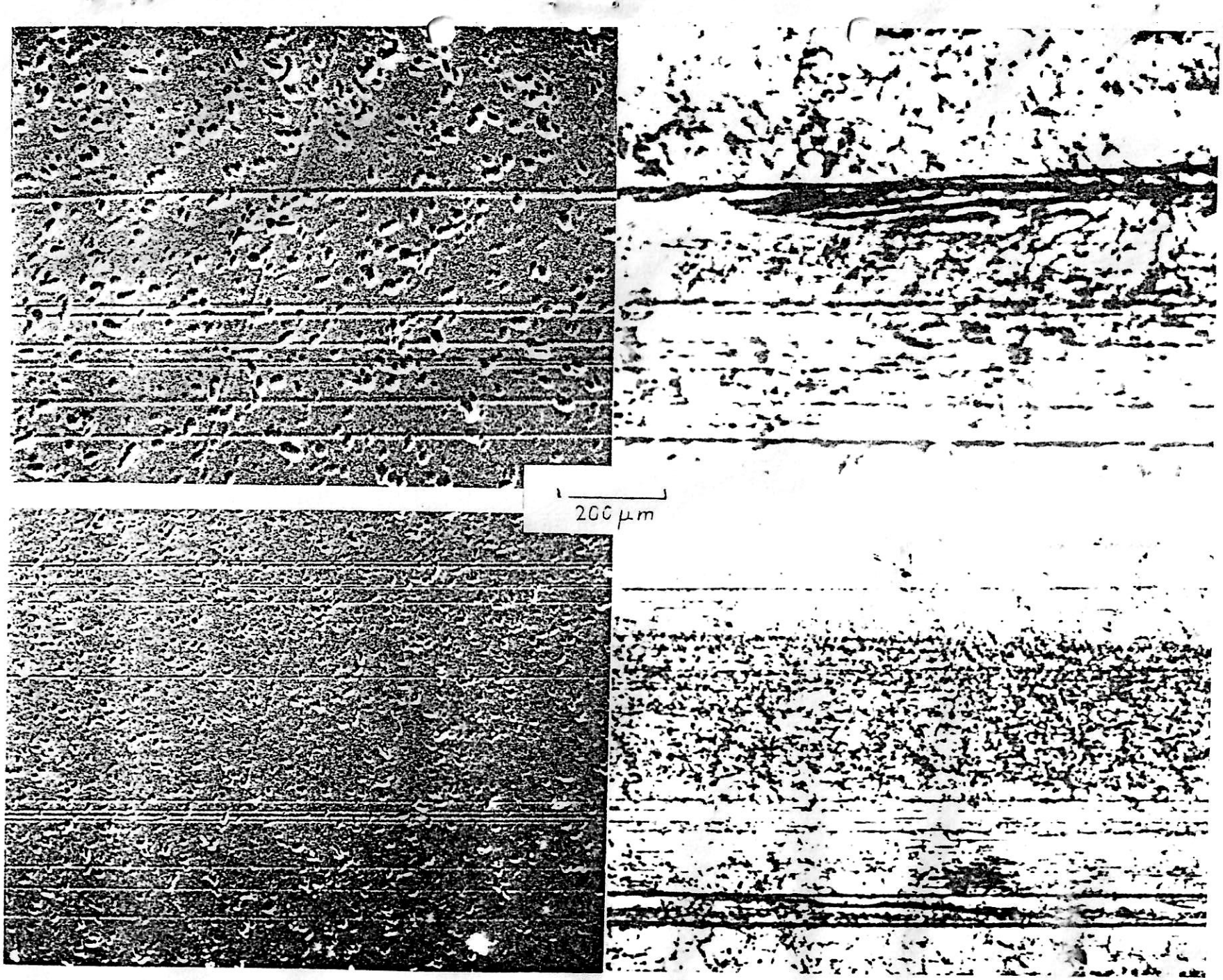

Fig. 7 Comparison etching pattern (left) – EBIC picture (right). Although the etching pattern is not good enough to reveal enough information it

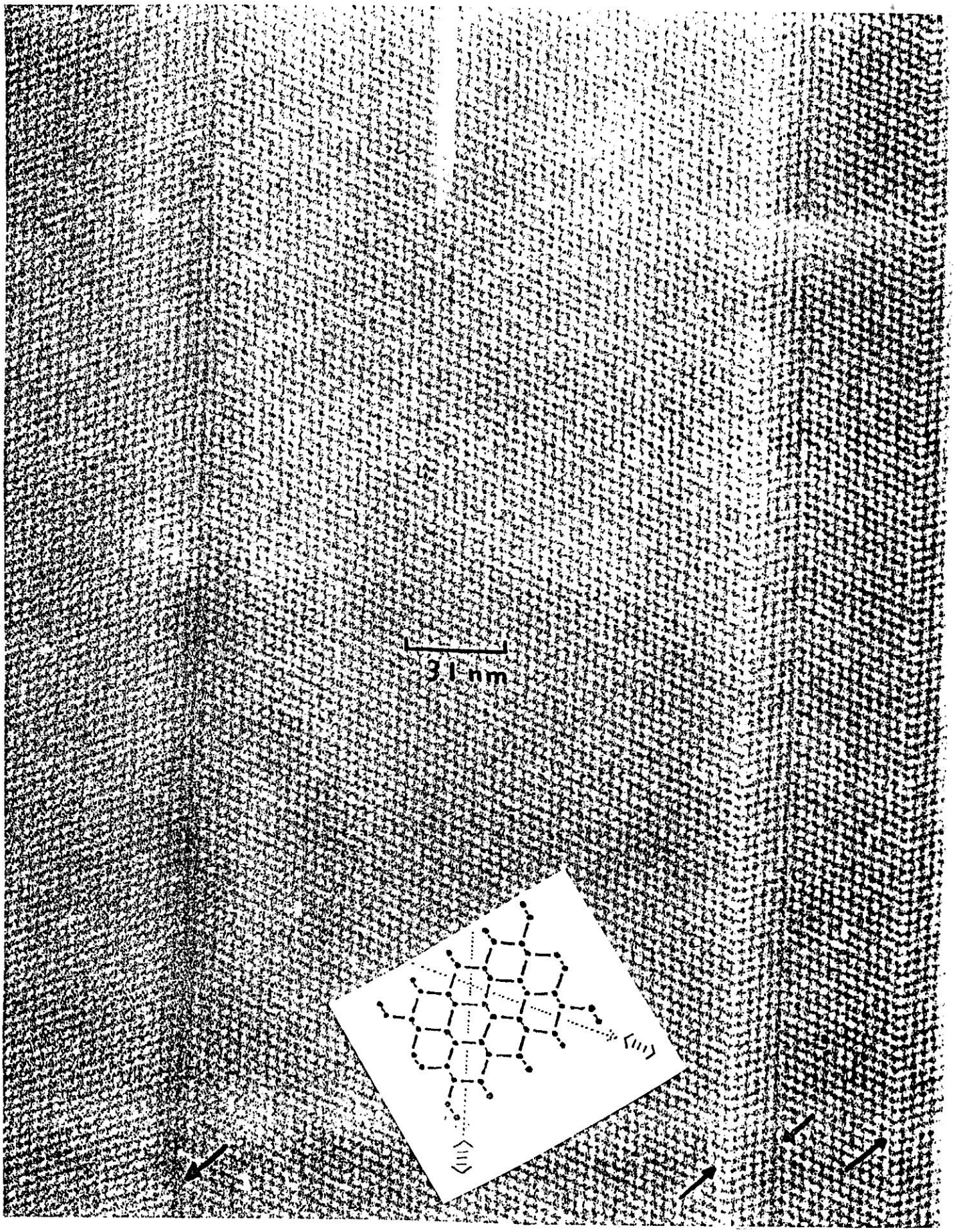

Fig. 8. Direct lattice image of coherent twin boundaries in Si ribbons. Boundaries marked with arrows.

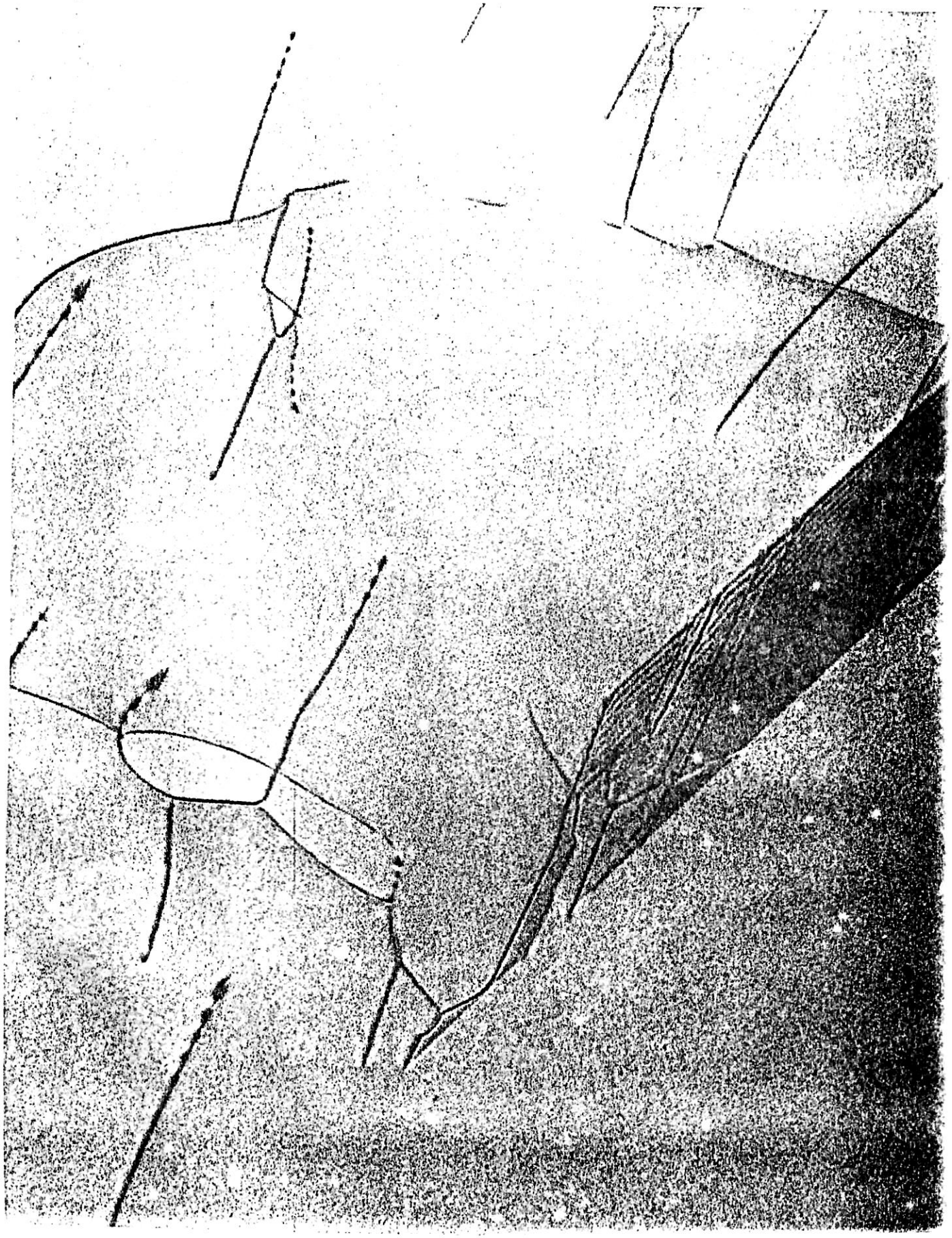

Fig. 9. Tip of microtwin ending in the specimen. Twinning dislocations and emitted dislocations are clearly

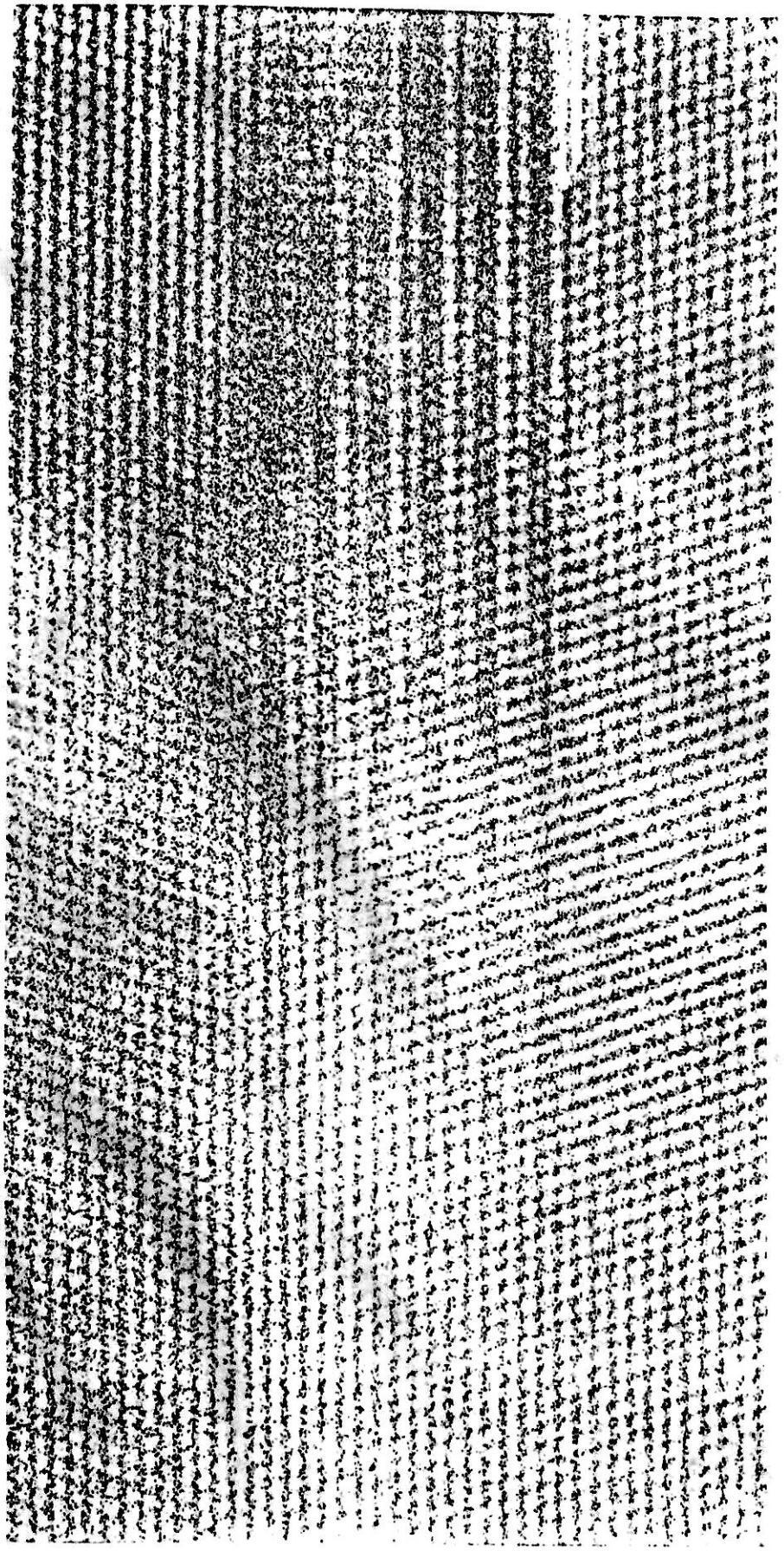

Fig. 10 Direct lattice image of incoherent twin boundary inclined in foil.

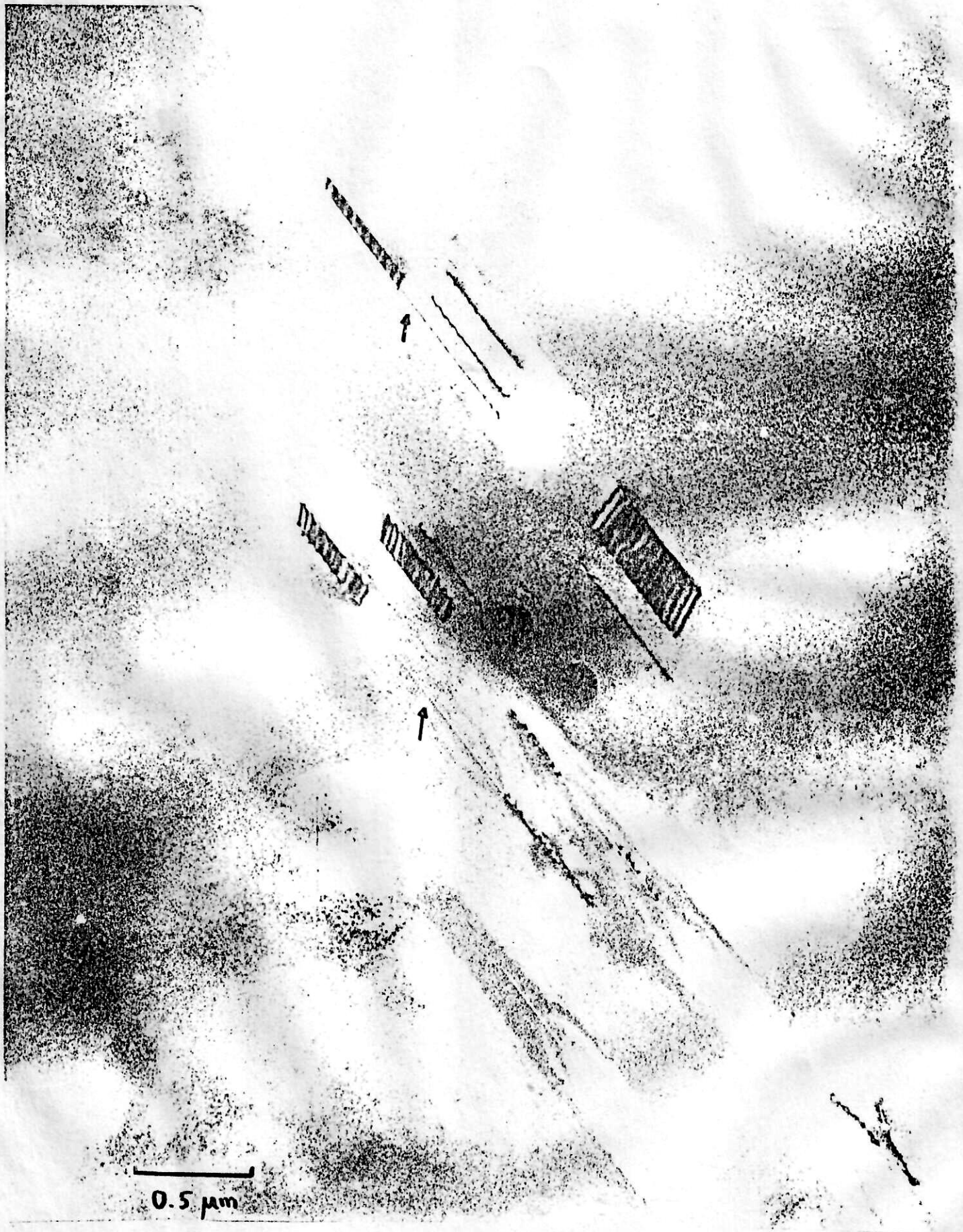

Fig. 11 Microtwins (marked by arrows and viewed exactly end-on) ending in the foil by emitting planar defects

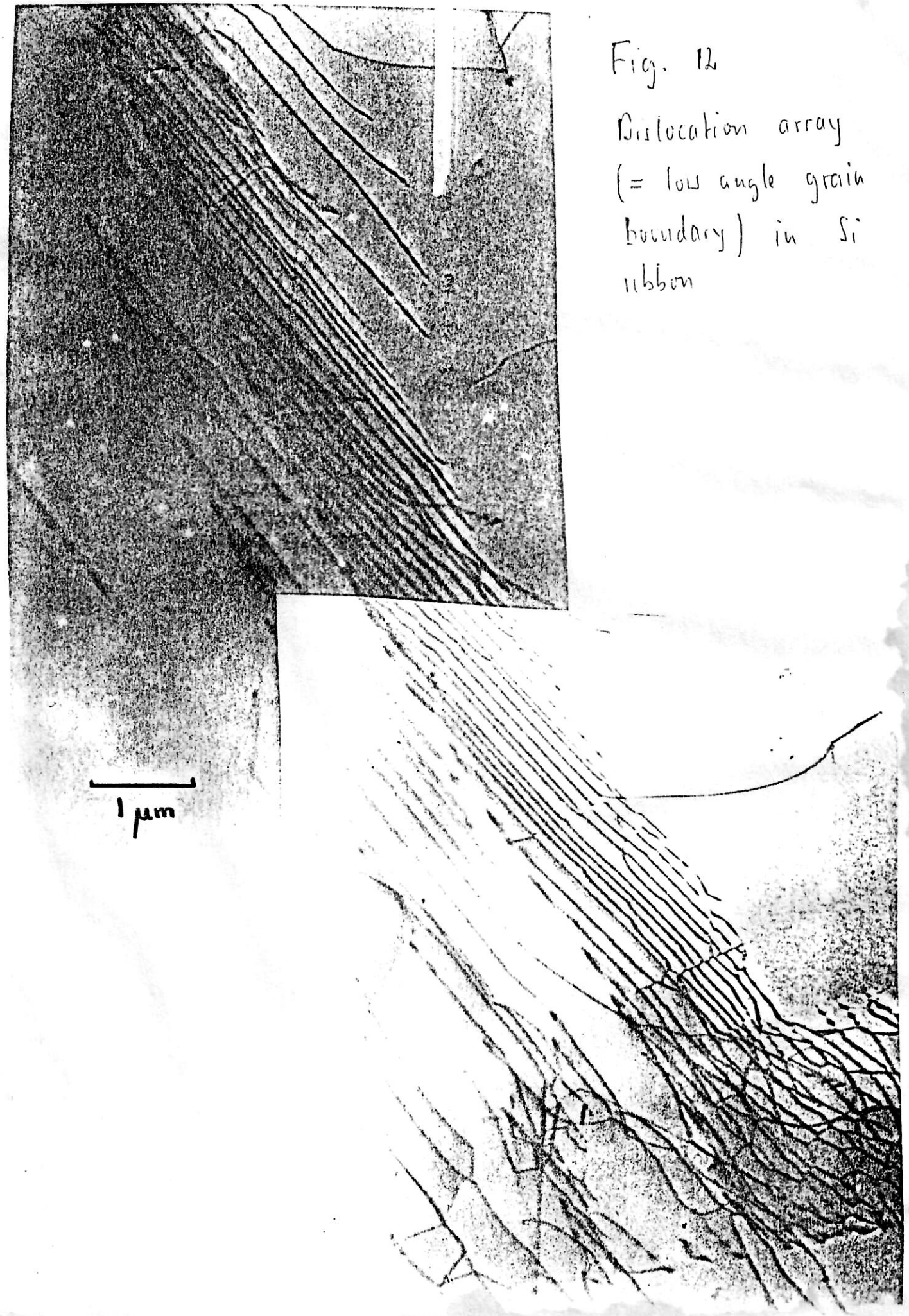

Fig. 12

Dislocation array (= low angle grain boundary) in Si ribbon